Electromagnetic Evaluation for Precaution against Electromagnetic Interference in Nuclear Power Plants

Jaeyul Choo, Dong-Jin Lee, Hyung Tae Kim, Daehee Kim, Youngdoo Kang, Hyun Shin Park, and Youngsik Cho

Department of Instrument, Control, and Electrical Systems, KINS, 34142, Daejeon, Korea (k728cjy@kins.re.kr)

Abstract: This paper represents the electromagnetic evaluation to avoid electromagnetic interference problems in a nuclear power plant using a mode-matching method. Using the mode-matching method in conjunction with the separation of variables, the superposition principle, and the Fourier transform, we perform the electromagnetic interpretation for three postulated topics: an open cabinet containing the digital instrumentation and control (I&C) modules when it is exposed to an external electromagnetic source, the axially-ruptured coaxial cable with multiple dielectrics, and the shorted cable trays between lateral walls. The examined results provide us with the useful information for avoiding the electromagnetic interference problem for the postulated cases.
Keyword: Mode-matching method, electromagnetic interference, nuclear power plant

1 Introduction

The equipment for instrumentation and control (I&C) in a nuclear power plant has been digitalized because the digital device provides cost-saving, extended functionality, and simplicity, etc[1]. In addition, the need to use wireless communication in a nuclear power plant has continually increased over time due to mobility and convenient access to communication networks[2]. However the digitalization of I&C equipment simultaneously causes the electromagnetic (EM) problems such as degradation and malfunction by external electromagnetic interference (EMI)[1][2]. To be more, the application of wireless communication to nuclear power plants poses an ongoing challenge because of the unwanted EMI caused by wireless devices, which would lead to detrimental malfunctions in adjacent equipment[1][2]. To avoid EM problems, it is required to electromagnetically evaluate the possible events. Thus we electromagnetically interpret the postulated EMI problems in the nuclear power plant using a mode-matching method. The evaluated results allows us to build the practical precaution against the postulated EMI problems.

In what follows, we will introduce the guidance applied to the EMI / EMS evaluation in a nuclear power plant as a perspective of the regulation. Afterwards, we will briefly explain the procedure of the mode-matching analysis for the EMI problems. We will then evaluate the EMI problems in the view of regulation using the various results computed by the mode-matching method.

2 Regulatory guidance for evaluating EMI problems in nuclear power plants

The EM evaluation of digital I&C equipment for safety functions is generally performed in terms of two characteristics: an EMI evaluation to verify that the radiated and conducted EMI of the equipment under test (EUT) is bounded by the allowable level, as well as an EMS evaluation to ensure that the EUT maintains the functionalities against the emitted and conducted EMI with the threshold level. Regulatory Guide (Reg. Guide) 1.180 published by the United States Nuclear Regulatory Commission is generally endorsed to evaluate EMI / EMS in nuclear power plants[3]. Herein we explain the categories of evaluation in [3] focusing on EMI / EMS problems by the radiated electric field.

2.1 EMI and EMS tests for radiated electric field

To evaluate the EMI and EMS problems related to the radiated electric field in nuclear power plants, [3] introduces RE102 and RS103 tests, respectively. In detail, [3] provides the allowable strength of the radiated electric field required to meet the acceptance criterion of the RE102 test. To satisfy this test, the measured strength of the electric field radiated from the EUT is lower than the allowable strength in Fig. 1. For RS103 test, [3] defines the susceptibility threshold

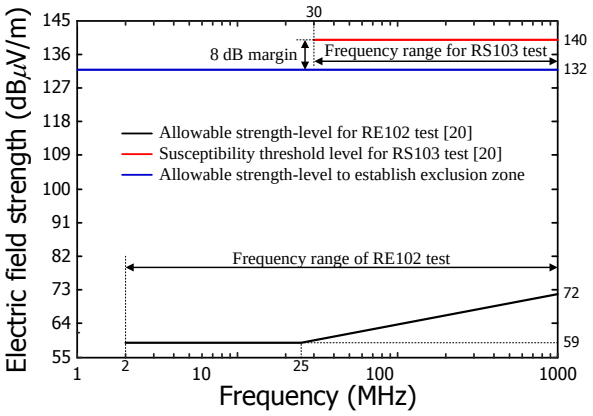

Fig. 1. Allowable strength and susceptibility threshold strength of the radiated electric field for RE102 and RS103 tests and evaluation of exclusion zone.

strength for the interference of the radiated electric field as 10 V/m (= 140 dBμV/m). In the case where the EUT functions and operates as designed during exposure to an interfering electric field with strength 10 V/m, we can confirm that the EUT satisfies the acceptance criterion of the RS103 test.

2.2 Exclusion zone

To protect digital I&C equipment from undesirable EM sources such as walkie-talkies and welding equipment, an exclusion zone is established as the minimum separation distance at which point portable EM sources should not be placed or approach the installed I&C equipment. The exclusion zone is determined by the regions in which the portable EM source has an electric field strength under 4 V/m (= 132 dBμV/m), which is considered the 8 dB margin to the recommended susceptibility threshold strength of 10 V/m (= 140 dBμV/m). Accordingly, the exclusion zone, which corresponds to the minimum separation distance (D) from the existing I&C equipment, is calculated as[3]

$$D = \frac{\sqrt{30EIRP}}{AE} = \frac{\sqrt{30P_TG_T}}{AE} \qquad (1)$$

where D is the minimum separation distance for the exclusion zone, $EIRP$ (= $P_T \times G_T$) is the equivalent isotropically radiated power of an external EM source, AE is the allowable strength of the electric field (= 4 V/m = 132 dBμV/m) , and P_T and G_T are the input power and the power gain of the external EM source, respectively.

As shown in (1), the exclusion zone with a large separation distance implies that the external EM source emits a strong electric field.

3 Mode-matching method

The mode-matching method, which is combined with the Fourier transform, the separation of variable, and the superposition principle, has been widely employed to solve the wave scattering problem rigorously[4][5]. We summarize the steps of the mode-matching method for the wave scattering problems in this paper as follows[4][5].

Step 1) Divide the scattering space into closed and open sub-regions.

Step 2) Represent the scattered fields in the closed and open sub-regions in terms of the Fourier series and transform, respectively.

Step 3) Enforce the boundary condition on the field continuities between the sub-regions.

Step 4) Apply the mode-matching technique to obtain the simultaneous equations for the Fourier series modal coefficients. If required, the residue calculus is utilized to perform the rapid-convergent integration.

Step 5) Check the convergence behavior of the series solutions to confirm the accuracy in computation after truncating the maximum mode number.

Step 6) Evaluate various EM characteristics for the wave scattering problem.

Note that the electric field is substituted with the potential in the Step 2, as well as the Dirichlet boundary conditions on the potential continuity and the Neumann boundary conditions on the normal derivative continuity are applied as boundary condition in Step 3 in the case of electrostatic problem.

4 Evaluation of EMI problems

Based on the investigated regulatory guidance in previous Section 2, we performed rigorously an EM evaluation of three postulated topics: the open cabinet containing the digital I&C modules when it is exposed to an external EM source, the axially-ruptured coaxial cable with multiple dielectrics, and the shorted cable trays between lateral walls. Note that the more detailed

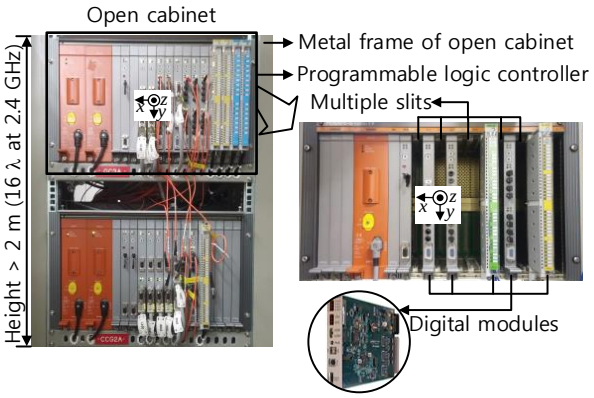

Fig. 2. Configuration of an open cabinet with inserted digital modules into multiple slits (front view).

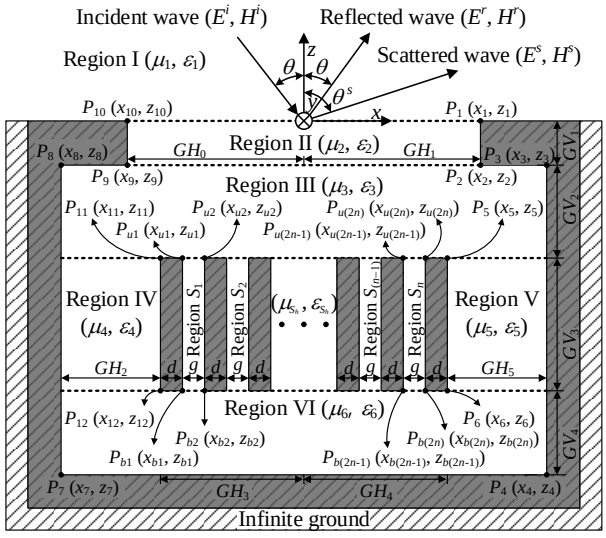

Fig. 3. Cross section of an open cabinet (top view).

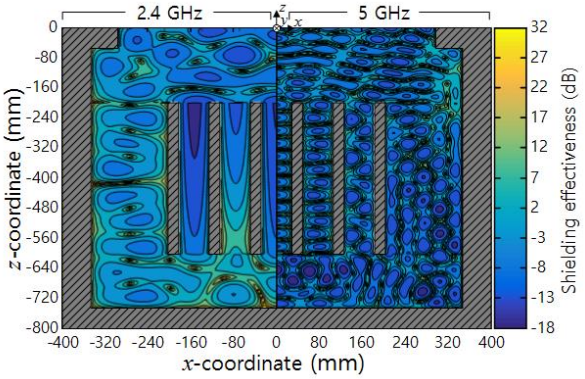

Fig. 4. SE_E at 2.4 GHz and 5 GHz when the number of inner slits is five. (GH_0 = GH_1 = 0.3 m, GH_2 = GH_5 = 0.15 m, GV_1 = 0.05 m, GV_2 = GV_4 = 0.15 m, GV_3 = 0.4 m, g = 0.0625 m, d = 7 / 480 m).

information on the mode-matching formulation and computed results for three cases can be seen in [6-9].

4.1 Open cabinet containing digital I&C modules

4.1.1 Structure of the open cabinet

Fig. 2 shows the open cabinet equipped with a programmable logic controller (PLC) in the metallic frame that manages the analog and digital input/output signals based on its logic algorithm. As shown in the right-hand pictures in Fig. 2, the PLC is composed of the digital modules between multiple slits on a metallic rack. To analyze the shielding performance of the cabinet, we simply model the digital modules of the PLC and the metallic frame as illustrated in Fig. 3 in assumption that the metallic cabinet is infinitely long along the y-axis. In addition, we assume that the metallic cabinet is buried in infinite ground to simplify the outer structure and exclude the influence from the surrounding objects. We also set the (n + 1) digital modules to be located at the center of the cabinet and simplified as conducting plates with thickness d and separation gap g. We herein consider that the external plane wave with the incident angle θ impinges on the cabinet and is then reflected at angle θ and scattered inside and outside the cabinet. With regard to the polarization of the incident, reflected, and scattered plane waves, it is assumed that the electric field is parallel to the y-axis (transverse electric (TE) to the plane of incidence). Thus, the incident and reflected plane waves are represented as follows:

$$E_y^i = e^{i(k_x x - k_z z)} \tag{2}$$

$$E_y^r = -e^{i(k_x x + k_z z)} \tag{3}$$

where $k_x = k_0 \sin\theta$, $k_z = k_0 \cos\theta$, and k_0 ($= \omega\sqrt{\mu_0 \varepsilon_0}$) is the wave number in free space.

Based on the simplified structure and the environmental assumption, we utilized the mode-matching method to analyze the open cabinet with digital modules.

4.1.2 Evaluation results

We examined both SE_E at 2.4 GHz and 5 GHz, which are the operating frequencies for IEEE 802.11 (Wi-Fi) and IEEE 802.15.4 (Wireless Hart) protocols, when the external plane wave has the incident angle of 0°. Fig. 4 shows the resulting distributions of shielding effectiveness for electric field (SE_E)[6] when the geometric parameters of the open cabinet with five slits

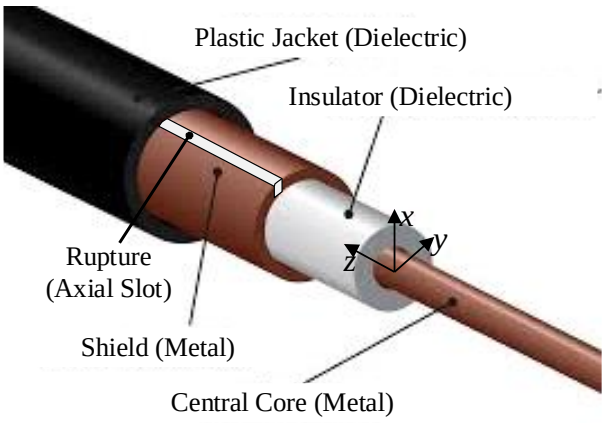

Fig. 5. Configuration of an axially-ruptured coaxial cable.

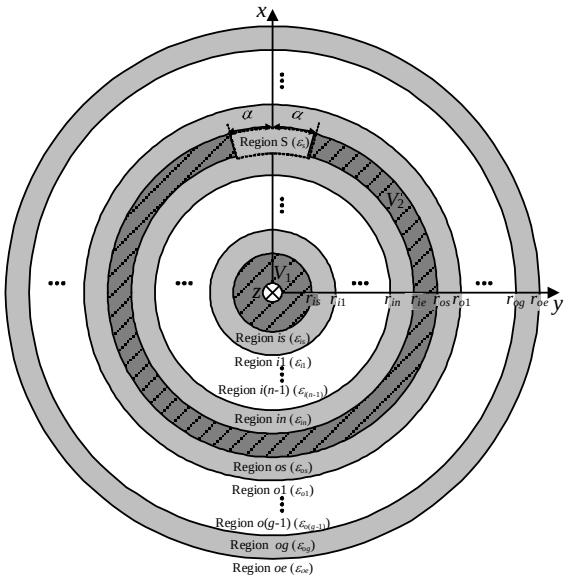

Fig. 6. Cross section of an axially-ruptured coaxial cable with multiple dielectrics.

are $GH_0 = GH_1 = 0.3$ m, $GH_2 = GH_5 = 0.15$ m, $GV_1 = 0.05$ m, $GV_2 = GV_4 = 0.15$ m, $GV_3 = 0.4$ m, $g = 0.0625$ m, and $d = 7 / 480$ m. Because of the symmetric distributions of SE_E with respect to the y–z plane, only half of the resulting distribution for each frequency is presented. In Fig. 4, the value of SE_E in each slit is low, which indicates that the protection from an electric field is more significantly considered. In addition, compared with the distribution of the SE_E at 2.4 GHz, the external plane wave at 5 GHz further penetrates slits between the digital modules. This result reveals that the precaution against an EMI problem should be taken before the external EM source with the high operating frequency is used around the cabinet related to the safety function.

4.2 Axially-ruptured coaxial cable with multiple dielectrics

4.2.1 Structure of axially-ruptured coaxial cable with multiple dielectrics

A coaxial cable is generally composed of a central metallic-core, an intermediate dielectric-insulator surrounded by a metallic-shield, and an outer dielectric-jacket as shown in Fig. 5. The coaxial cable transmits the signal and power effectively using the EM field confined to the dielectric-insulator between the central metallic-core and the metallic-shield. Thus the physical and material deformation of the coaxial cable possibly causes the variation in EM characteristics. Especially, in case that the metallic-shield of the coaxial cable is damaged, it possibly occurs that the undesired EMI / EMS problems between the coaxial cable and existing equipment

Fig. 6 illustrates the cross section of the ruptured coaxial cable, which is composed of a central metallic-core with a potential V_1, inner dielectric-layers of (n + 1) for insulators as regions *is* and *i*1–*in*, a metallic shield having a single layer with a potential V_2, and outer dielectric-layers of (g + 1) as a jacket as regions *os* and *o*1–*og*. We assume that the coaxial cable, which is infinitely extended in the z-direction, is ruptured in the form of an axial slot with slot angle 2α, which is depicted as region *s*, and surrounded by free space, which is illustrated as region *oe*. More specifically, the dielectric constant and radius for each region are defined as ε_R and r_R (R = *is*, *i*1, ⋯ , *in*, *s*, *os*, *o*1, ⋯ , *og*, and *oe*), respectively, in Fig. 6.

We electrostatically solved the EMI problem caused by the axially-rupture of a coaxial cable with multiple dielectrics using a mode-matching method[8].

4.2.2 Evaluation results

Fig. 7 shows the computed electric-field strength distributions compared with the susceptibility threshold level of 10 V/m in the RS103 test, and the allowable strength of 4 V/m, required to estimate the exclusion zone. As expected, the electrical field leaks toward the outside of the coaxial cable through the axial slot. This leaky electrical field may cause an EMI problem to adjacent objects. In addition, we confirmed that the inner dielectric with high permittivity makes the radiating electric field strong whereas the outer dielectric with high permittivity weakens the radiating electric field. These results provide us with important information on the types of dielectric that are required

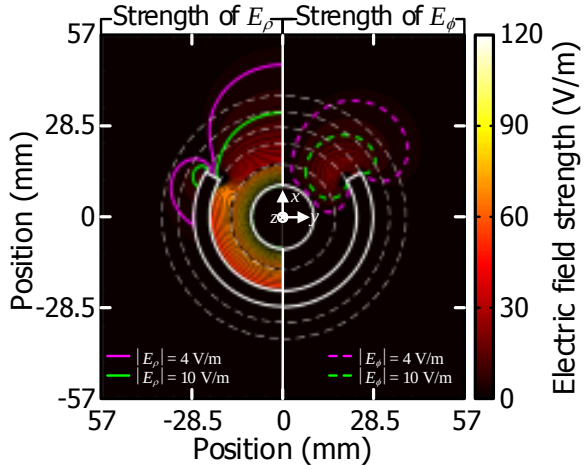

Fig. 7. Computed electrical-field distribution.
where $\varepsilon_{is} = \varepsilon_{i1} = \varepsilon_s = \varepsilon_{os} = \varepsilon_{o1} = \varepsilon_{oe} = \varepsilon_0$. n = 1, q = 1, r_{is} = 10 mm, r_{i1} = 16.505 mm, r_{ie} = 23.01 mm, r_{os} = 28 mm, r_{o1}= 33 mm, r_{oe} = 38 mm, slot angel 2α = 120°, V_1 = 1 V, V_2 = 0 V, and $\varepsilon_0 \approx 8.854 \times 10^{-12}$.

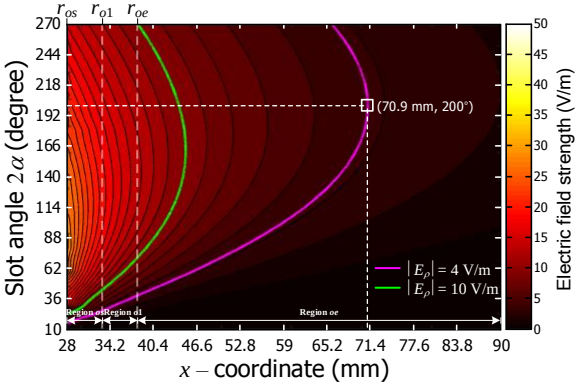

Fig. 8. Strength of electrical field E_ρ at ϕ = 0° in terms of x-coordinate while varying slot angle 2α.
where n = 1, q = 1, r_{is} = 10 mm, r_{i1} = 16.505 mm, r_{ie} = 23.01 mm, r_{os} = 28 mm, r_{o1}= 33 mm, r_{oe} = 38 mm, V_1 = 2 V, V_2 = 0 V, and $\varepsilon_{is} = \varepsilon_{i1} = \varepsilon_s = \varepsilon_{os} = \varepsilon_{o1} = \varepsilon_{oe} = \varepsilon_0 \approx 8.854 \times 10^{-12}$.

in order for the inner and outer dielectrics to alleviate EMI.

As shown in Fig. 8, it is seen that the electric field strength of the ρ–component (E_ρ) leaking through the slot is fairly dominant at ϕ = 0° (on the x-axis). Thus, we investigated the strength of E_ρ at ϕ = 0° while the slot angle 2α varied from 10° to 270° using the same geometric and material parameters to those in Fig. 7. The investigated result as a function of the x-coordinate from r_{os} and the slot angle 2α is shown in Fig. 8, where the contours of equivalent E_ρ of 4 V/m and 10 V/m are highlighted. From Fig. 8, it is observed that the strength of E_ρ at the same position on the x-axis increases as the slot angle 2α increases, and then decreases after the maximum E_ρ. In practice, estimating the minimum separation distance for the exclusion zone is important from a regulatory perspective when the leaky electrical field has a maximum strength. From the investigated results in Fig. 8, we therefore recommend that the digital I&C equipment susceptible to EMI maintains a separation distance of 70.9 mm (as marked by the symbol □) from the axially-ruptured coaxial cable to avoid the adverse EMI effect.

4.3 Shorted cable trays between lateral walls

4.3.1 Configuration of shorted cable trays between lateral walls

The cable trays have been employed to protect and isolate the power and communication cables from physical and EM damage and fire attacks in industrial facilities such as a nuclear power plant. Because the short accident caused by the inner leaky cable electromagnetically affects nearby equipment we evaluate EMI from the shorted cable trays without grounding.

Fig. 9 illustrates a cross section of two enclosed-cable trays surrounded by multilayer dielectrics with the lateral conducting walls of 0 V. The potentials V_1 and V_2 are applied to two enclosed-cable trays with the widths w_1 and w_2, respectively, and the separating distance s. The surrounding dielectrics are specifically divided into three different regions, which are regions u_k with ε_{uk} (k = 1, 2, 3, ···) for the upper dielectrics, regions b_t with ε_{bt} (t = 1, 2, 3, ···) for the bottom dielectrics, and regions 1–3 with ε_1, ε_2, and ε_3 for the dielectrics adjacent to two enclosed-cable trays. The lateral walls stand apart from the closed-cable trays with distances d_1 and d_2.

We electrostatically interpreted the complicated structure in Fig. 9 effectively using a mode-matching method while the material and geometric parameters change

4.3.2 Evaluation results

Fig. 10 shows the electric field strength of x-component (E_x) and z-component (E_z) for the shorted cable trays with the applied potentials of V_1 = –1 and V_2 = 1 where the surrounding layers are filled with air (ε_r = 1) and the geometry parameters are $w_1 = s = w_2$ = 5 m, h_{u1} = 1 m, and $d_1 = d_2$ = 10 m. The electric fields are normalized by the absolute potential difference $|V_2 - V_1|$ between two cable trays. Due to the symmetry with respect to y-z plane, the result in Fig. 10 is seen to be symmetrical distributions. In Fig. 10(a), the equivalent contours of E_x are dense between two

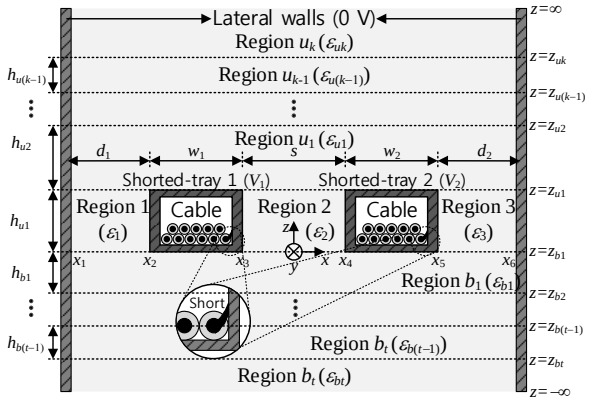

Fig. 9. Cross section of the shorted enclosed-cable trays in the multilayer dielectrics.

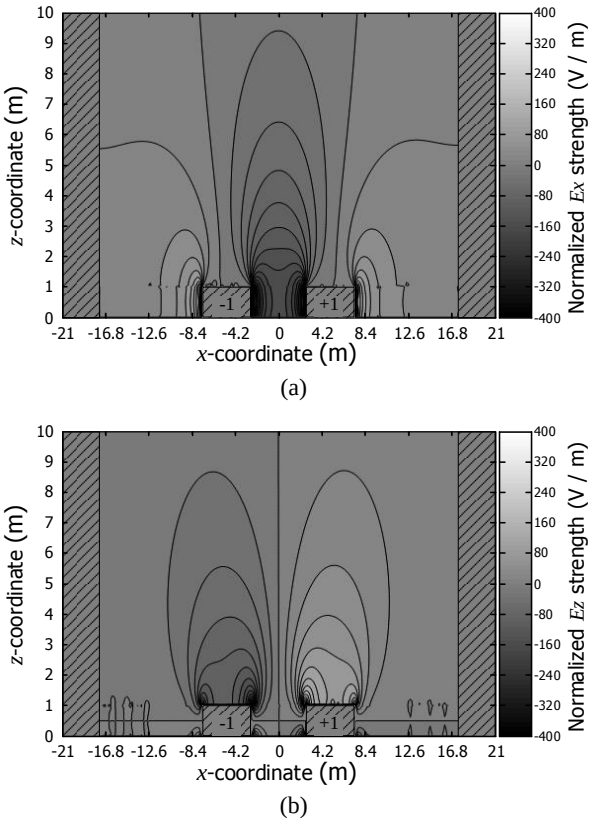

Fig. 10. Electric field distribution and strength of enclosed-cable trays surrounded with air: (a) x–component (E_x) and (b) z–component (E_z) of electric field strength.
where $w_1 = s = w_2 = 5$ m, $h_{u1} = 1$ m, $d_1 = d_2 = 10$ m, $V_1 = -1$, and $V_2 = 1$

enclosed-cable trays, which means the strong electric field and EM coupling. In addition, the equivalent contours of E_z in Fig. 10(b) are tilted to the direction of the lateral walls that indicates the distances d_1 and d_2 are also the important factors influencing on electric field.

5 Conclusion

We evaluated the postulated EMI problems that are the open cabinet containing the digital I&C modules, the axially-ruptured coaxial cable with multiple dielectrics, and the shorted cable trays between lateral walls. Before evaluating EM characteristics for each case, we investigated regulatory guidance for a nuclear power plant on EMI and EMS to prevent undesired EMI. We then explained the mode-matching method that is employed to analyze the postulated EMI problems in our work. Based on the investigated regulatory guide, we performed the EM evaluations on the three cases using a mode-matching method. Considering the investigated regulatory guidance, we derived the useful information to avoid EMI using the investigated electrical field distribution in change of geometric and material parameters. The derived evaluation results would provide instructive information to alleviate the EMI problem in a nuclear power plant

Acknowledgement

This work was supported by the Nuclear Safety Research Program through the Korea Foundation of Nuclear Safety (KOFONS), granted financial resource from the Nuclear Safety and Security Commission (NSSC), Republic of Korea (1305003-0315-SB130).

References

[1] Guidelines for electromagnetic interference testing of power plant equipment: Revision 4 to TR-102323, EPRI, Palo Alto, CA, 2013.

[2] Implementation guideline for wireless networks and wireless equipment condition monitoring, EPRI, Palo Alto, CA, 2009.

[3] Guidelines for evaluating electromagnetic and radio-frequency interference in safety-related instrumentation and control systems, Rev. 1, U. S. NRC, Oct. 2003.

[4] H. J. Eom, Wave Scattering Theory, Springer Verlag, Berlin, 2001.

[5] H. J. Eom, Electromagnetic Wave for Boundary-Value Problem, Springer Verlag, Berlin, 2004.

[6] J. Choo, J. Choo, and Y. H. Kim, "Shielding effectiveness of open cabinet containing digital modules using ferrite sheet," IEEE Transactions on Magnetics, 2017 (In press).

[7] J. Choo, C. H. Jeong, and J. Choo, "Transverse electric scattering of open cabinet in nuclear power plants," IEEE Antennas Wireless Propagation Letter,

Vol. 15, pp. 1204-1207, 2016

[8] J. Choo, H. S. Park, Y. Cho, Y. H. Kim, and H. J. Choi, "Quasi-static analysis of slotted coaxial cable," 2017 IEEE AP-S Symposium on Antennas and Propagation, San Diego, USA, Jul. 9~14, 2017.

[9] J. Choo, H. T. Kim, H. S. Park, and C. H. Jeong, "Electrostatic analysis of a short accident in cable trays for intelligent pressure transmitters," IU-Journal of Electrical & Electronics Engineering. Vol. 16, No. 2, pp. 2039-2045, 2016.